LAWRENCE
LIVERMORE
NATIONAL
LABORATORY

LLNL-PROC-769422

The effect of pre-plasma formed under the non-local transport conditions on the interaction of the ultra-high intensity laser with a solid target

J. Nikl, M. Jirka, M. Kucharik, M. Holec, M. Vranic, S. Weber

March 12, 2019

SPIE Optics + Optoelectronics 2019
Prague, Czech Republic
April 1, 2019 through April 4, 2019

Disclaimer

The effect of pre-plasma formed under the non-local transport conditions on the interaction of the ultra-high intensity laser with a solid target

J. Nikl[a,b], M. Jirka[a,b], M. Kucharík[b], M. Holec[c], M. Vranic[d], and S. Weber[a]

[a] *ELI Beamlines, Institute of Physics, Czech Academy of Sciences, 18221 Prague, Czech Republic*
[b] *Faculty of Nuclear Sciences and Physical Engineering, Czech Technical University, 11519 Prague, Czech Republic*
[c] *Center for Applied Scientific Computing, Lawrence Livermore National Laboratory, 94551 Livermore, California, USA*
[d] *GoLP/Instituto de Plasmas e Fusão Nuclear, Instituto Superior Técnico, Universidade de Lisboa, 1049-001 Lisbon, Portugal*

ABSTRACT

The pre-plasma effects have been extensively studied experimentally and numerically and techniques for suppressing the pre-pulse are known widely. However, the increasing availability of the (multi-)PW-class laser systems enables to perform experiments with ultra-high laser intensities. The simulations of the pre-plasma formation and the effect on the main laser pulse must be reconsidered, since the systems are always limited in the contrast available and the created pre-plasma affects the interaction considerably. Our recent investigation of the topic revealed that the non-local transport of energy going beyond the paradigm of the diffusive approximation plays an important role in the process. An over-critical plateau is formed, where the main pulse is absorbed partially before reaching the solid target. Moreover, strong filamentation of the laser field occurs in the plasma. This effect is studied further by the means of the hydrodynamic simulations of the pre-plasma followed by the kinetic simulations of the interaction of the main pulse.

Keywords: pre-plasma, ultra-high intensity, non-local transport, radiation hydrodynamics

1. INTRODUCTION

New frontiers are opening to the laser plasma research as the intensities available at the laser systems increase worldwide.[1] With (multi-)PW-class laser systems available, the laser–plasma interaction (LPI) enters even the ultra-relativistic regime as the intensity tops $\gtrsim 1 \cdot 10^{22}\,\mathrm{W/cm^2}$. However, new challenges must be faced, since all laser systems are subject to a limited contrast. The intensity of the pre-pulse even with best effort gets far beyond the ionization threshold of the target, leading to formation of the pre-plasma.[2] The importance of the effect of the pre-plasma on the experimental results is well-known for lower intensities.[3] Although, the effect on the experiments with ultra-intense lasers is far less explored and neglected in the theory usually. Therefore, we investigate these phenomena in detail by combination of the appropriate numerical methods, where the hydrodynamic description is used for the pre-pulse simulation and the kinetic particle model for the main pulse of the laser. The relevance of this research is not limited to the ultra-intense lasers at world-leading laser facilities such as ELI Beamlines,[4–7] APOLLON[8] or SULF.[9] In the broader context, it points out that the pre-pulse interaction should be reconsidered for applications like ion acceleration[10] or shock ignition,[11] because discrepancies between the results with the classical heat diffusion model and the non-local radiation transport are observed. Following the previous effort with low-Z materials,[12] also the results with a mid-Z material are presented.

Further author information: (Send correspondence to J. Nikl)
J. Nikl: E-mail: jan.nikl@eli-beams.eu
S. Weber: E-mail: stefan.weber@eli-beams.eu, Telephone: +420 266 051 317

2. MODELS

The problem of interest is the interaction of a laser pulse with a massive solid target. To resemble the real conditions, where only a limited contrast is available, the full temporal profile of the laser pulse is modelled as a flat-top pre-pulse (with a small initial ramp, see Sec. 3) with the laser intensity I_{pre} and the Gaussian main pulse with the peak intensity I_L. The particular values used in the simulations are given in Sec. 3 together with the rest of the numerical setup. However, it must be mentioned that the length of the pre-pulse τ_{pre} is of the order of nanoseconds, while the length of the main pulse τ_L is less than one picosecond. The complexity of the laser–target interaction with such laser pulse requires to combine both methods, the hydrodynamic and particle description. The former is used for the simulation of the pre-pulse as described in Sec. 2.1, while the latter is applied to the main pulse according to Sec. 2.2.

In order to provide a better insight into the physics of the pre-plasma, the problem is formulated as one-dimensional, i.e. the laser pulse is modelled as a plane wave. The hydrodynamic simulations are performed in 1D and extended in the transversal direction defining the initial condition for the 2D PIC (Particle-In-Cell) simulation. However, the symmetry of the problem is broken there as shown in Sec. 3 manifesting the instabilities occurring in the pre-plasma. The 1D formulation of the problem then gives rather a statistical impression about these transient phenomena involved in the interaction.

2.1 Hydrodynamic model

The collisionally dominant regime of the laser–plasma interaction can be modelled in terms of the hydrodynamic approach in a good approximation. The plasma is described as an inviscid two-temperature fluid governed by the Euler equations, which are solved numerically. In particular, the Lagrangian code PETE has been used for this purpose, which offers fully non-local radiation transport among other features.[13] In the approximation of the gray-body and with absorptive processes dominating over the scattering in the laser plasma,[14] the equation of radiation transport takes the form:

$$\frac{1}{c}\frac{\partial I}{\partial t} + \vec{n}\cdot\nabla I = \rho\kappa(S - I)\ , \tag{1}$$

where $I = I(t, \vec{x}, \varphi, \theta)$ is the radiation intensity defined at time t, space coordinate $\vec{x}$, polar angle φ and azimuthal angle θ. The unit vector $\vec{n}$ points in the direction of propagation, i.e. it takes the form $\vec{n} = (\cos\varphi, \sin\theta\sin\varphi, \cos\theta\sin\varphi)^T$ in the three-dimensional case. The rest of the symbols are defined as follows: c the speed of light in vacuum, ρ the mass density and S the black-body source function. The last but not least, κ is the average gray-body total opacity, which presents an interpolation between the Planck and Rosseland opacities depending on the non-locality of the transport.[13] In particular the measure of the non-locality is the reduced radiation flux $f_R = |q_R| / (c\epsilon_R)$ in this case, i.e. the radiation flux $q_R = \iint I\cos\varphi\sin\varphi\,\mathrm{d}\varphi\,\mathrm{d}\theta$ normalized to the product of the radiation energy calculated as $c\epsilon_R = \iint I\sin\varphi\,\mathrm{d}\varphi\,\mathrm{d}\theta$. This presents an improvement over our previous simulations[12] and reflects better the energy dependency of the opacity in the simulations with mid-Z targets used in Sec. 3, where the radiation transport becomes the dominant energy transport mechanism in the plasma.

2.2 Particle-in-cell model

We have performed 2D PIC simulations in the open-source code EPOCH[15] to asses the role of the created pre-plasma on laser pulse propagation. The EPOCH code is a relativistic electrodynamic PIC code enabling to perform numerical simulations in which both, the radiation reaction[16] and electron-positron pair creation via the Breit-Wheeler process,[17] are included.

The PIC simulation is initialized from the data computed by the hydrodynamic model. However, the prohibitive computational demands of the simulation effectively disable simulation of the progressing ionization of the target of the solid density. Fortunately, the process of ionization is very rapid for the laser intensities considered and does not play a vital role in the full physical scenario. Therefore, the full ionization is considered for the mass density profiles originating from the hydrodynamic part. Likewise, heating of the electrons during the pre-pulse is negligible compared to the energies obtained by the electrons in the interaction with the main pulse. Hence, the initial electron temperature in the PIC simulation is set to zero uniformly.

3. NUMERICAL RESULTS

The numerical simulations of the full laser interaction were performed with a solid Aluminium target with the initial temperature $T_0 = 0.03\,\mathrm{eV}$ and density $\rho_0 = 2.7\,\mathrm{g/cm^3}$. The laser pulse is modelled as a plane wave with the temporal profile consisting of the two parts, the pre-pulse and the main pulse, as described in Sec. 2. The pre-pulse has a flat-top profile of the total length $\tau_{pre} = 6\,\mathrm{ns}$ with the intensity $I_{pre} = 1 \cdot 10^{12}\,\mathrm{W/cm^2}$ with an initial half-Gaussian ramp of the length 600 ps and equal FWHM (Full-Width-at-Half-Maximum). The main pulse following the pre-pulse had Guassian profile with FWHM width $\tau_L = 150\,\mathrm{fs}$ and the peak intensity $I_L = 1 \cdot 10^{23}\,\mathrm{W/cm^2}$, where the excellent contrast 10^{11} was considered to mimic the expected parameters of the L4 laser system at ELI Beamlines.[5,7] Accordingly, the laser wavelength (in vacuum) was set to $\lambda_0 = 1.05\,\mu\mathrm{m}$ corresponding to the fundamental frequency of the Nd:glass laser $1/\tau_0 = 2.855 \cdot 10^{14}\,\mathrm{s^{-1}}$.

The hydrodynamic simulations were performed with the geometrical computational mesh spanning from $-100\,\mu\mathrm{m}$ to $0\,\mu\mathrm{m}$ with 1000 computational cells and the geometrical factor 0.992 (the mesh is geometrically denser towards the frontal surface). For the laser absorption, a full wave-based laser absorption algorithm was used.[18] The equation-of-state for Aluminium was taken from the SESAME database[19,20] (material id: 3720) interpolated by the HerEOS library.[21] The model of the flux-limited heat conduction was applied with the heat flux limiter set to 0.05 of the free streaming flux.

In our 2D PIC simulations we studied interaction of a laser pulse with the created pre-plasma for the case with the non-local radiation transport and without it. The simulations were performed without Radiation–Reaction model for the moment, but a comparison with the simulations including this model is planned for the nearest future. The simulation box of dimensions $10\,\mu\mathrm{m} \times 400\,\mu\mathrm{m}$ was resolved with $600 \times 24,000$ cells. The periodic boundary conditions for the electromagnetic field were applied following the assumption of the one-dimensional formulation of the problem. The fully ionized plasma composed of free electrons and aluminium ions is represented by 10 macro-particles per cell for each specie. The longitudinal profile of the plasma density were taken from the output of the presented hydrodynamic simulations and extended in the transverse direction. The simulation domain spanned over the interval from $-200\,\mu\mathrm{m}$ to $200\,\mu\mathrm{m}$ in the coordinate system of the hydrodynamic simulation, where the center of the laser pulse was initialized at the position $245\,\mu\mathrm{m}$ at the beginning of the simulation.

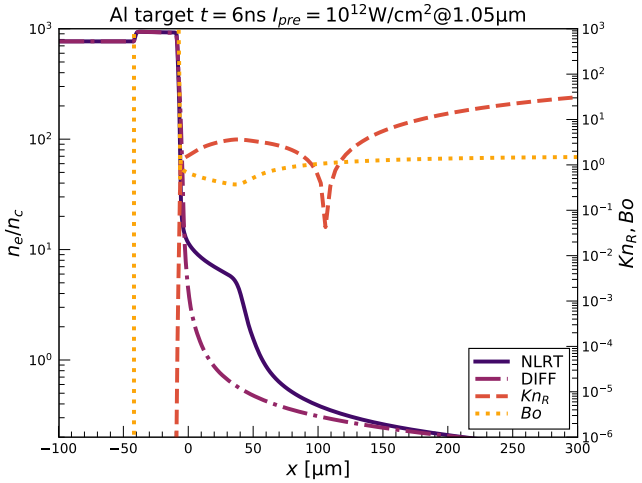

Figure 1. The spatial profile of the electron density n_e at the end of the pre-pulse ($t = 6$ ns). The curve "NRLT" presents the results with the non-local radiation transport and the curve "DIFF" with only the heat diffusion. The radiation Knudsen number Kn_R and the Boltzmann number Bo are plotted for the case with the radiation transport.

The electron density profiles normalized to the non-relativistic critical density $n_c = 1.011 \cdot 10^{21}\,1/\mathrm{cm^3}$ resulting from the hydrodynamic simulations are shown in Figure 1. These profiles then served as the initial condition of the PIC simulations with cut-off at $0.2\,n_c$ as marked in the plot. The difference between the two cases considered is immediate, the non-local transport of radiation gives rise to the over-dense plasma plateau

in the interval from $-5\,\mu m$ to $35\,\mu m$ approximately. This structure is known as the double-ablation-front (DAF) and appears in the laser plasma naturally as consequence of the local equilibrium between the radiation transport of energy and the hydrodynamic work.[22,23] As can be recognized from the radiation Knudsen number $Kn_R = 1/(\rho\kappa)\,\mathrm{d}(\ln \epsilon_R)/\,\mathrm{d}x$, the photons remain considerably non-local even after entering this area and efficiently transport the energy deposited in the vicinity of the critical plane by the laser deep into the plasma. This energy flux is compensated by the expansion of the plasma fluid as reflected by the nearly flat profile of the Boltzmann number $Bo = 5/2(p_e + p_i)|u|\,/(\sigma T_R^4)$, where p_e and p_i are the electron and ion pressures respectively, u is the single-fluid velocity, σ the Stefan-Boltzmann constant and T_R the radiation temperature related to the radiation energy as $\epsilon_R = 4\sigma/c\,T_R^4$. The characteristic DAF profile is then formed as a consequence of this quasi-equilibrium. The regime of moderate Kn_R observed in this zone is the most difficult for description, because the classical diffusion approximation is not valid there and the non-local description consistent with the diffusion in the limit of low Kn_R must be used instead.[13]

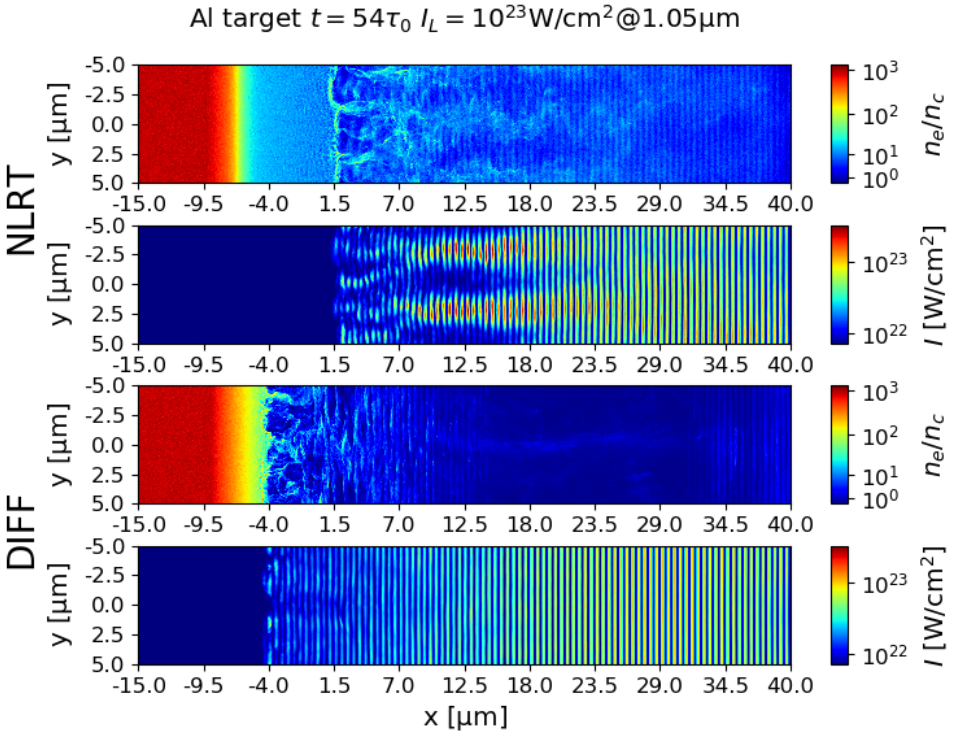

Figure 2. The spatial plasma profiles in 2D PIC simulations at time $t = 54\tau_0 \doteq 189\,\mathrm{fs}$. The simulations with the non-local radiation transport denoted as "NLRT" are in the upper half and the simulations with only the heat diffusion denoted as "DIFF" are in the lower half. The first row in each part is the electron density n_e normalized to the non-relativistic critical density n_c. The second row is the intensity of the electromagnetic field.

The results of the 2D PIC simulations are presented in Figure 2 for time $t = 189\,\mathrm{fs}$ (measured from the beginning of the PIC simulation), i.e. short before the laser pulse hits the solid target. A qualitative difference is clearly visible there. In the case with the DAF structure (denoted as "NLRT"), the laser is being strongly filamented due to the over-dense pre-plasma before reaching the target. In addition, the electromagnetic wave-packet of the laser pulse is being slowed down due to the decreasing group velocity. In contrast, the simulation without the over-dense pre-plasma does not exhibit almost any filamentation before the interaction with the solid target and the group velocity remains nearly unaltered. The laser crosses the pre-plasma interacting with it only negligibly, where only small protuberances close to the surface of the target are observed.

The total energy of the electromagnetic field ε_L in Figure 3 supports the statements of the previous paragraph. Due to the negligible plasma density in the right part of the computational domain, the laser pulse enters

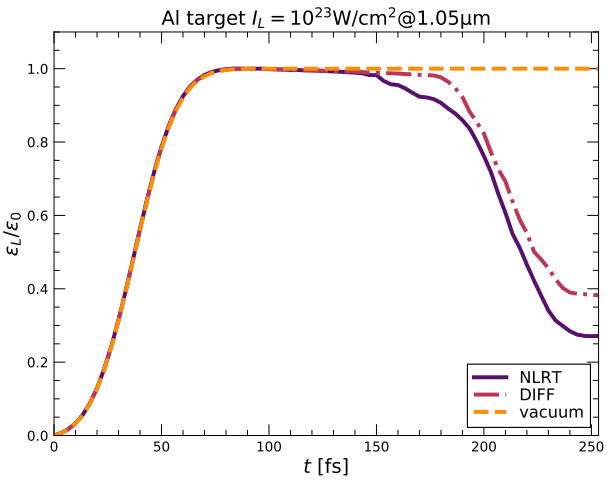

Figure 3. The time dependency of the electromagnetic field energy ε_L normalized to the maximum value ε_0. The curve "NRLT" presents the results with the non-local radiation transport and the curve "DIFF" with only the heat diffusion. The reference profile in absence of the plasma is denoted as "vacuum".

the domain without any observable attenuation and nearly reaches the maximal energy of the reference pulse propagating in vacuum. A considerable absorption can be observed from 150 fs approximately when the pulse enters the denser plasma. At time of the Figure 2 ($t = 189$ fs), the difference between the simulations with and without the non-local radiation transport makes 6.5 % already (normalized to the reference simulation). At the end of the simulation, the curves saturate indicating that the interaction ends there too. The total reflectivity of the target then can be understood as the ratio of the actual energy of the field to the reference one. Following this definition, the reflectivity with the non-local radiation transport is 27 % and 38 % without it. This shows that the absorption is significantly higher with the over-dense pre-plasma in addition to the apparent filamentation.

4. CONCLUSIONS

Summarizing the results of Sec. 3, it becomes clear that the pre-plasma certainly cannot be neglected even for the ultra-relativistic interaction of a laser with an initially solid target. Moreover, the approximation of only the heat diffusion without the radiation transport is not sufficient for the description of the pre-pulse. The non-local radiation transport results in formation of an over-dense plasma plateau, which strongly filaments the laser wave and increases the overall absorption by 11 % approximately. This effect agrees with our previous results for low-Z materials.[12] All together, the studies disprove the usual shortcoming that the pre-plasma profile can be modelled as a simple exponential profile for the purposes of the PIC simulations of ultra-intense lasers that are becoming available today. Undoubtedly, the problem considered a plane wave initially, so the quantitative nature of the results is limited, because the effects of focusing and diffraction are not taken into account, but the qualitative differences are immediate. The full 2D/3D simulations of the laser interaction with the target remain topics of the future research.

ACKNOWLEDGMENTS

This work has been supported by the project High Field Initiative (HiFI) (CZ.02.1.01/0.0/0.0/15_003/0000449), Advanced research using high intensity laser produced photons and particles (ADONIS) (CZ.02.1.01/0.0/0.0/16_019/0000789) and ELI Tools for Advanced Simulation (ELITAS) (CZ.02.1.01/0.0/0.0/16_013/0001793), project CZ.02.1.01/0.0/0.0/16_019/0000778, all from European Regional Development Fund; Czech Technical University grant SGS16/247/OHK4/3T/14 and Czech Science Foundation project 18-20962S. This project has received funding from the Eurofusion Enabling Research Project No. ENR-IFE19.CEA-01. This work was performed under the auspices of the U.S. Department of Energy by Lawrence Livermore National Laboratory under Contract DE-AC52-07NA27344.

REFERENCES

[1] Danson, C., Hillier, D., Hopps, N., and Neely, D., "Petawatt class lasers worldwide," *High Power Laser Sci. Eng.* **3**, e3 (2015).

[2] Esirkepov, T. Z., Koga, J. K., Sunahara, A., Morita, T., Nishikino, M., Kageyama, K., Nagatomo, H., Nishihara, K., Sagisaka, A., Kotaki, H., Nakamura, T., Fukuda, Y., Okada, H., Pirozhkov, A. S., Yogo, A., Nishiuchi, M., Kiriyama, H., Kondo, K., Kando, M., and Bulanov, S. V., "Prepulse and amplified spontaneous emission effects on the interaction of a petawatt class laser with thin solid targets," *Nucl. Instrum. Meth. A* **745**, 150–163 (2014).

[3] Rosen, M. D., Phillion, D. W., Rupert, V. C., Mead, W. C., Kruer, W. L., Thomson, J. J., Kornblum, H. N., Slivinsky, V. W., Caporaso, G. J., Boyle, M. J., and Tirsell, K., "The interaction of 1.06 micron laser radiation with high Z disk targets," *Phys. Fluids* **22**, 2020 (1979).

[4] "The Extreme Light Infrastructure project: ELI Beamlines." http://www.eli-beams.eu.

[5] Rus, B., Bakule, P., Kramer, D., Naylon, J., Thoma, J., Green, J. T., Antipenkov, R., Fibrich, M., Novak, J., Batysta, F., Mazanec, T., Drouin, M. A., Kasl, K., Base, R., Peceli, D., Koubikova, L., Trojek, P., Boge, R., Lagron, J. C., Vyhlidka, S., Weiss, J., J, C., Hrebicek, J., Hribek, P., Durak, M., Polan, J., Koselja, M., Korn, G., Horacek, M., Horacek, J., Himmel, B., Havlíček, T., Honsa, A., Korouš, P., Laub, M., Haefner, C., Bayramian, A., Spinka, T., Marshall, C., Johnson, G., Telford, S., Horner, J., Deri, B., Metzger, T., Schultze, M., Mason, P., Ertel, K., Lintern, A., Greenhalgh, J., Edwards, C., Hernandez-Gomez, C., Collier, J., T, D., Gaul, E., Martinez, M., Frederickson, C., Hammond, D., Malato, C., White, W., and Houzvicka, J., "ELI-Beamlines: development of next generation short-pulse laser systems," in [*Research Using Extreme Light: Entering New Frontiers with Petawatt-Class Lasers II*], Korn, G. and Silva, L. O., eds., *Proc. SPIE* **9515**, 951501 (2015).

[6] Korn, G. and Silva, L. O., eds., [*Research Using Extreme Light: Entering New Frontiers with Petawatt-Class Lasers III*], *Proc. SPIE* **10241** (2017).

[7] Weber, S., Bechet, S., Borneis, S., Brabec, L., Bučka, M., Chacon-Golcher, E., Ciappina, M., DeMarco, M., Fajstavr, A., Falk, K., Garcia, E.-R., Grosz, J., Gu, Y.-J., Hernandez, J.-C., Holec, M., Janečka, P., Jantač, M., Jirka, M., Kadlecova, H., Khikhlukha, D., Klimo, O., Korn, G., Kramer, D., Kumar, D., Lastovička, T., Lutoslawski, P., Morejon, L., Olšovcová, V., Rajdl, M., Renner, O., Rus, B., Singh, S., Šmid, M., Sokol, M., Versaci, R., Vrána, R., Vranic, M., Vyskočil, J., Wolf, A., and Yu, Q., "P3: an installation for high-energy density plasma physics and ultra-high intensity laser-matter interaction at ELI-Beamlines," *Matter Rad. Extremes* **2**, 149 (2017).

[8] Zou, J., Le Blanc, C., Papadopoulos, D., Chériaux, G., Georges, P., Mennerat, G., Druon, F., Lecherbourg, L., Pellegrina, A., Ramirez, P., Giambruno, F., Fréneaux, A., Leconte, F., Badarau, D., Boudenne, J., Fournet, D., Valloton, T., Paillard, J., Veray, J., Pina, M., Monot, P., Chambaret, J., Martin, P., Mathieu, F., Audebert, P., and Amiranoff, F., "Design and current progress of the Apollon 10 PW project," *High Power Laser Sci. Eng.* **3**, e2 (2015).

[9] Gan, Z., Yu, L., Li, S., Wang, C., Liang, X., Liu, Y., Li, W., Guo, Z., Fan, Z., Yuan, X., Xu, L., Liu, Z., Xu, Y., Lu, J., Lu, H., Yin, D., Leng, Y., Li, R., and Xu, Z., "200 J high efficiency Ti:sapphire chirped pulse amplifier pumped by temporal dual-pulse," *Opt. Express* **25**(5), 5169 (2017).

[10] McKenna, P., Carroll, D., Lundh, O., Markey, K., Bandyopadhyay, S., Batani, D., Evans, R., Jafer, R., Kar, S., Neely, D., Quinn, M., and Redaelli, R., "Effects of front surface plasma expansion on proton acceleration in ultraintense laser irradiation of foil targets," *Laser Part. Beams* **26**, 591 (2008).

[11] Batani, D., Baton, S., Casner, A., Depierreux, S., Hohenberger, M., Klimo, O., Koenig, M., Labaune, C., Ribeyre, X., Rousseaux, C., Schurtz, G., Theobald, W., and Tikhonchuk, V., "Physics issues for shock ignition," *Nucl. Fusion* **54**, 054009 (2014).

[12] Holec, M., Nikl, J., Vranic, M., and Weber, S., "The effect of pre-plasma formation under nonlocal transport conditions for ultra-relativistic laser-plasma interaction," *Plasma Phys. Contr. F.* **60**(4), 044019 (2018).

[13] Nikl, J., Holec, M., Zeman, M., Kuchařík, M., Limpouch, J., and Weber, S., "Macroscopic laser-plasma interaction under strong non-local transport conditions for coupled matter and radiation," *Matter Rad. Extremes* **3**, 110–126 (2018).

[14] Zeldovich, Y. B. and Raizer, Y. P., [*Physics of Shock Waves and High-Temperature Hydrodynamic Phenomena*], Dover Publications, New York (2002).

[15] Arber, T. D., Bennett, K., Brady, C. S., Lawrence-Douglas, A., Ramsay, M. G., Sircombe, N. J., Gillies, P., Evans, R. G., Schmitz, H., Bell, A. R., and Ridgers, C. P., "Contemporary particle-in-cell approach to laser-plasma modelling," *Plasma Phys. Contr. F.* **57**(11), 113001 (2015).

[16] Vranic, M., Martins, J. L., Fonseca, R. A., and Silva, L. O., "Classical radiation reaction in particle-in-cell simulations," *Comp. Phys. Comm.* **204**, 141 (2016).

[17] Ridgers, C., Kirk, J., Duclous, R., Blackburn, T., Brady, C., Bennett, K., Arber, T., and Bell, A., "Modelling gamma-ray photon emission and pair production in high-intensity laser-matter interactions," *J. Comput. Phys.* **260**, 273–285 (2014).

[18] Nikl, J., Kuchařík, M., Limpouch, J., Liska, R., and Weber, S., "Wave-based laser absorption method for high-order transport–hydrodynamic codes," *Adv. Comput. Math.* (2019). Accepted.

[19] Group, T., "SESAME report on the Los Alamos equation-of-state library," Tech. Rep. Tech. Rep. LALP-83-4, Los Alamos National Laboratory, Los Alamos (1983).

[20] Lyon, S. P. and Johnson, J. D., "SESAME: The Los Alamos national laboratory equation of state database," Tech. Rep. LA-UR-92-3407, Los Alamos National Laboratory, Los Alamos (1992).

[21] Zeman, M., Holec, M., and Váchal, P., "HerEOS: A framework for consistent treatment of the Equation of State in ALE hydrodynamics," *Comput. Math. Appl.* (2018). Accepted.

[22] Sanz, J., Betti, R., Smalyuk, V., Olazabal-Loumé, M., Drean, V., Tikhonchuk, V., Ribeyre, X., and Feugeas, J., "Radiation hydrodynamic theory of double ablation fronts in direct-drive inertial confinement fusion," *Phys. Plasmas* **16**, 082704 (2009).

[23] Drean, V., Olazabal-Loumé, M., Sanz, J., and Tikhonchuk, V., "Dynamics and stability of radiation-driven double ablation front structures," *Phys. Plasmas* **17**, 122701 (2010).